Kinetic and Modeling Studies of the Mechanism of the Dehydrogenation of $Mg(BH_4)_2$ to $Mg(B_3H_8)_2$

Sunil Shrestha[1], McKinley A. Prager[2], Kazuumi Fujioka, Rui Sun, and Craig M. Jensen[*]

Department of Chemistry, University of Hawaii at Manoa, Honolulu, HI 96822

KEYWORDS

Hydrogen storage, magnesium borohydride, kinetics, kinetic modeling, mechanism

ABSTRACT

Since its discovery over 15 years ago, the reversible dehydrogenation of $Mg(BH_4)_2$ to $Mg(B_3H_8)_2$ has remained one of the more intriguing hydrogen-cycling systems. While the mechanism of this reaction has been the subject of a good deal of speculation and computational studies, prior to this work it had not been probed through kinetic studies. Previous reports of the dehydrogenation of $Mg(BH_4)_2$ to $Mg(B_3H_8)_2$ have not included kinetic studies. The present studies have shown that the dehydrogenation of $Mg(BH_4)_2$ to $Mg(B_3H_8)_2$ is suppressed by hydrogen pressure indicating that the rate-limiting step in this process involves hydrogen elimination. Computational modeling of kinetic data obtained from monitoring the hydrogen elimination from $Mg(BH_4)_2$ to $Mg(B_3H_8)_2$ under static vacuum over a range of temperatures supports that the dehydrogenation occurs through a reversible three-step process in which the elimination of hydrogen from the $[B_3H_{10}]^-$ intermediate is rate limiting. A mechanism involving the low energy transfer of neighboring BH_3 groups is proposed to account for the formation of $[B_3H_8]^-$ at relatively low temperatures.

INTRODUCTION

Magnesium borohydride, $Mg(BH_4)_2$, (**1**) has been extensively investigated for over 20 years as a potential hydrogen storage material due to its high gravimetric hydrogen density and thermodynamically favorable hydrogen cycling compatibility [1-20]. This interest was piqued by the observation of the direct hydrogenation of magnesium diboride, MgB_2 (**2**) to **1** and the demonstration of the cycling of 11.7 wt% hydrogen [7]. This still stands as the highest gravimetric hydrogen capacity that has ever been experimental demonstrated for any material. However, this hydrogen cycling was accomplished at the extreme reaction conditions of 900 bar and 450 ˚C. More recently, there have been many reports that the reaction conditions required for both the dehydrogenation of **1** [10-15] and the hydrogenation of **2** to **1** [16,17] and can be significantly reduced by the addition of selected additives. Nonetheless overcoming the extremely slow kinetics of the reversible release of hydrogen in the solid state remains a daunting challenge that must be met before **1** can be utilized as a practical hydrogen storage material.

Less extensive hydrogen cycling between **1** and $Mg(B_3H_8)_2$ (**3**) (Equation 1), was first demonstrated by Chong *et al.* [10] These studies established that reversible dehydrogenation of **1**

$$3Mg(BH_4)_2 \leftrightharpoons Mg(B_3H_8)_2 + 2MgH_2 + 2H_2 \qquad (1)$$

was possible in the solid-state under moderate conditions (dehydrogenation 200 °C; hydrogenation, 250 °C/120 bar H_2 pressure hydrogen). While the reversible dehydrogenation of **1** to **3** has a more limited, maximum cycling capacity of 2.5 wt% H_2, the finding of reversibility at moderate conditions has led to considerable investigation and speculation concerning the mechanism of this process [18-20].

Early seminal studies of borohydrides established key patterns of reactivity which are undoubtedly essential components of the mechanism of the dehydrogenation of **1** to **3**. The reaction between metal borohydrides and binary metal hydrides/borane species is well known, as seen in Equation 2 [21-23]. There is also a consensus among investigators that the first step of conversion

$$MBH_4 \rightarrow MH + BH_3 \quad (2)$$

of **1** to **3** involves a borohydride-borane coupling as shown in Equation 3 [20, 24-27].

$$MBH_4 + BH_3 \longrightarrow MB_2H_7 \quad (3)$$

The formation of $[B_3H_8]^-$ can then be completed by the addition of another equivalent of BH_3 and elimination of H_2. However, it is ambiguous as to the sequence of the BH_3 addition and H_2 elimination as shown in Scheme 1.

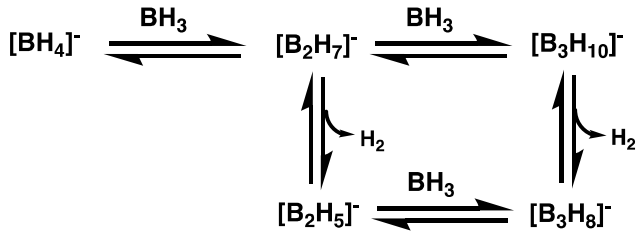

Scheme 1. Potential pathways for the reaction from $[BH_4]^-$ to $[B_3H_8]^-$.

Prior experimental studies mechanistic studies for the formation of $[B_3H_8]^-$ from $[BH_4]^-$ have been carried out in solution using either diborane or a BH_3 adduct as a reactant [24-27]. Chen *et al.* showed that $[B_3H_8]^-$ can be synthesized through the reaction of $[BH_4]^-$ with 2 equivalents of BH_3-THF [26]. They propose that the reaction proceeds by a mechanism involving the initial coupling of $[BH_4]^-$ and BH_3 to give $[B_2H_7]^-$. The B2 intermediate then reacts with a second equivalent of BH_3 to form the $[B_3H_{10}]^-$ intermediate before undergoing dehydrogenation to $[B_3H_8]^-$ (Scheme 1) [26]. Gaines *et al.* prepared $[B_3H_8]^-$ by the reaction of $[BH_4]^-$ and diborane,

B_2H_6 [28]. They propose a similar mechanism in which $[B_3H_8]^-$ is formed directly from $[B_3H_{10}]^-$ via a H_2 elimination [28]. Beall *et al*. has suggested that the hydrogen elimination is most likely the endothermic, rate-limiting step [25].

A recent computational study by Johnson *et al.* that investigated ground-state stabilities of different borane species calculated $[B_3H_{10}]^-$ as a lower energy intermediate than $[B_2H_5]^-$, thus indicating that BH_3 addition occurs first [20]. An alternative mechanism has been proposed by Wan *et al.* [19] However, they propose that the preferred reaction pathway involves the $[B_3H_9]^{2-}$ dianion, which is not commonly considered as a component in the chemistry of lower anionic boranes [29]. While the previous experimental and computational studies have revealed important insights into the reaction pathway between **1** and **3**, a full understanding of the mechanistic details of the process in the solid state requires information about the kinetic parameters governing this process. In order to obtain this information, we have carried out kinetic studies and modeled our findings using line-fitting analysis in order to elucidate a valid mechanism for the reversible dehydrogenation of **1** to **3**. Such analysis has allowed for the determination of the rate constant and activation energy (Ea) associated with the elementary step(s) for the forward and reverse reactions, thus revealing which step is rate-limiting in the case of a multi-step reaction.

1. EXPERIMENTAL

General Considerations. All sample preparations were carried out either in an argon glovebox or using standard Schlenk techniques under argon. All kinetic experiments were carried out with a calibrated *Suzuki Shokan PCT-2SDWIN* Sieverts-type apparatus. ^{11}B NMR spectroscopy was performed on *Varian Unity Innova* 500 MHz spectrometer with ^{11}B chemical shifts referenced to $BF_3{\cdot}OEt_2$ (δ = 0 ppm) at 20 °C and ^1H referenced to TMS (δ = 0 ppm). A relaxation delay of 10

seconds was used for all ^{11}B analyses with a 90° pulse width of 10 μs. For ^{11}B analysis, powders were typically dissolved in a 2:1 mixture of D_2O and THF. All samples were analyzed within 45 minutes of sample dissolution. Powder X-ray Diffraction (PXRD) were obtained on a Bruker D8 Advance diffractometer with a 3 kW CuKα source and a LynxEye XE detector in Bragg–Brentano parafocusing geometry, mounted on a 9-position automated sample changer using an air free Bruker Si-wafer mount. A 0.020 mm Ni filter was used to reduce CuKβ radiation. Powder scans were conducted over a range of 3–83 degrees with a step size of 0.02 degrees and an exposure time of 1 s per step.

Synthesis of Magnesium Borohydride. Synthesis of $Mg(BH_4)_2$ was prepared according to the procedure by Zanella *et. al.* [30]. Di-*n*-butylmagnesium (10 mL, Sigma Aldrich, 1M solution in heptane) was slowly added dropwise to borane-dimethylsulfide complex (18 mL, Acrōs Organics, 2M in toluene) and the solution was stirred for a minimum of two hours at room temperature during which a white precipitate formed. This solid was filtered through a Schlenk frit, washed twice with toluene, and dried for 12 hours *en vacuo* at room temperature followed an additional at 75°C for 12 hours. The resulting white powder was found by PXRD analysis to be primarily γ-$Mg(BH_4)_2$ with a small amount of α-$Mg(BH_4)_2$. ^{11}B NMR (128 MHz, $2D_2O$:1THF) δ = − 42 ppm (m), ^{1}H NMR (400 MHz, D_2O); δ = − 0.30 ppm (m).

Isothermal Dehydrogenation Kinetic Measurements. Samples (50 mg, 0.93 mmol) of $Mg(BH_4)_2$ were added into a fixed volume reactor and attached onto the PCT instrument line where both reactor and line were evacuated. Samples were heated to the prescribed temperature. Pressure readings were recorded every 10 seconds. The amount of hydrogen released during the desorption

process was determined from the pressure difference in the calibrated volume after the measurements were complete.

Hydrogen Back Pressure Experiments. Samples (100 mg, 1.86 mmol) of $Mg(BH_4)_2$ were added into a fixed volume reactor and attached onto the PCT instrument line where both reactor and line were evacuated. In addition to a blank experiment in which no hydrogen pressure was introduced, 20 bar H_2 was introduced in a second run prior to heating. Samples were heated to the prescribed temperature. Pressure readings were recorded every 10 seconds. The amount of hydrogen released during the desorption process was determined from the pressure difference in the calibrated volume after the measurements were complete.

Computational Methods. The final kinetic model is modelled for the three coupled, reversible reactions, with the ordinary differential equation (ODE) solved with an Euler first-order integrator. The reactions are assumed to be first order with respect to each species. A variable timestep was used to ensure concentrations stay non-negative with a maximum step size of 0.4 seconds. Initially, no other species are present except for 9.26×10^{-4} mol of $Mg(BH_4)_2$. The python package *lmfit* (https://ui.adsabs.harvard.edu/abs/2016ascl.soft06014N) is used to iteratively update the rates $K = (k_{1f},k_{1r},k_{2f},k_{2r},k_{3f},k_{3r})$ to minimize between the difference between the ODE predicted H_2 concentrations and the measured H_2 concentrations, using the default least-squares algorithm. Since the parameter space of K is large, multiple initializations of K values (K_0) are chosen from a stochastic Monte Carlo sampling from rates as low as 10^{-4} to as high as 10^{20} for one of the reactions (with units $[mol^{-1} \times hr^{-1}]$ or $[mol^{-2} \times hr^{-1}]$ depending on the total reaction order). Each K_0 will result in an optimized K_{opt} and after aggregating hundreds of them, those K_{opt} corresponding

to a small difference between the ODE predicted H_2 concentrations and the measured H_2 concentrations are selected for Arrhenius plots. K_{opt} are further filtered out by the Arrhenius plots where those corresponding to large R^2 values and out of the range of chemical intuitions are omitted.

2. RESULTS AND DISCUSSION

Kinetic Monitoring of the Dehydrogenation of $Mg(BH_4)_2$ to $Mg(B_3H_8)_2$

Previous reports of the dehydrogenation of **1** to **3** have not included kinetic studies. In order to determine rate constants and mechanistic insights the hydrogen elimination from **1** to **3** under static vacuum over a range of temperatures was monitored as a function of time. Below 200 °C, the formation of **3** is exceedingly slow. It has been previously reported that between 200 and 250 °C, $[B_3H_8]^-$ is the sole product of the dehydrogenation. While above 250 °C, the dehydrogenation is no longer selective for the formation of $[B_3H_8]^-$ and thus complicates reaction kinetics. Therefore, meaningful data could only be collected over the very limited range of temperatures of 200-250 °C. Isotherms were collected at 10 °C increments for 19 hours as seen in Figure 1. The decay of

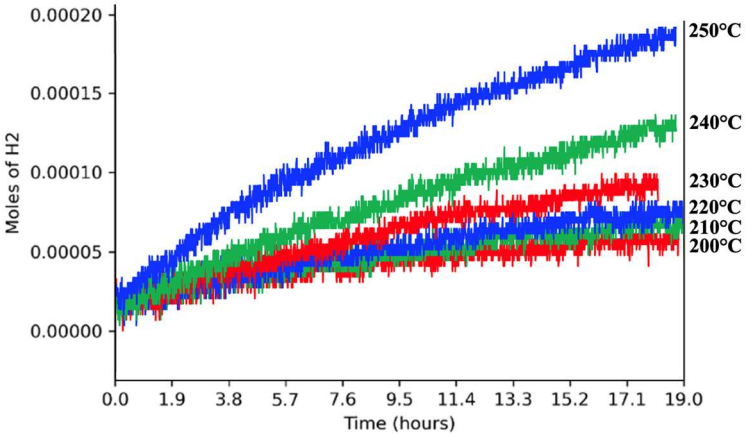

Figure 1. PCT isotherms generated during the dehydrogenation of $Mg(BH_4)_2$ at **(a)** 200 °C **(b)** 210 °C **(c)** 220 °C **(d)** 230 °C **(e)** 240 °C **(f)** 250 °C.

the rate of hydrogen elimination exhibits roughly Langmuir behavior. The $^{11}B\{^1H\}$ NMR spectra of the $[BH_4]^-/[B_3H_8]^-$ mixture obtained after 19 hours of heating at the prescribed temperatures are shown in Figure 2. Table 1 summarizes the relative integrated signal intensity of $[B_3H_8]^-$ and

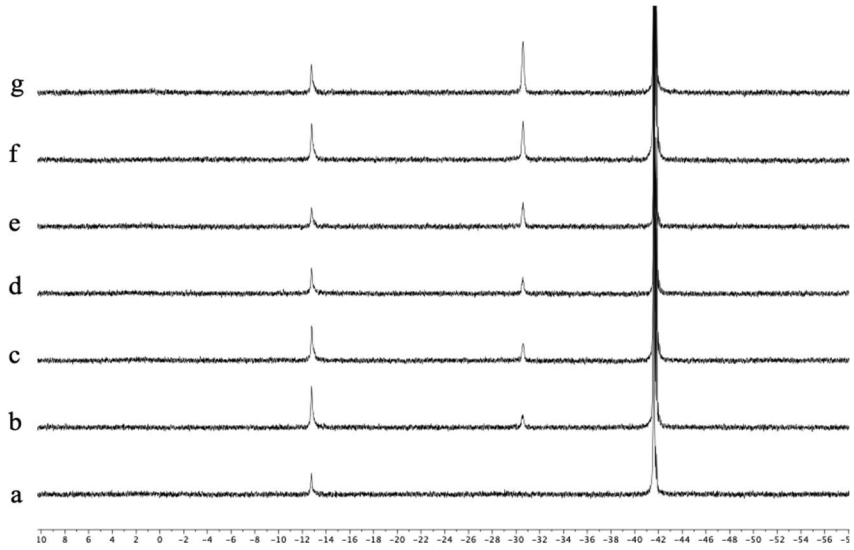

Figure 2. $^{11}B\{^1H\}$ NMR spectra of $Mg(BH_4)_2$ at **(a)** 23 °C and after dehydrogenating for 19 h at **(b)** 200 °C **(c)** 210 °C **(d)** 220 °C **(e)** 230 °C **(f)** 240 °C **(g)** 250 °C.

Table 1. Relative amounts of $[BH_4]^-$ and $[B_3H_8]^-$ after dehydrogenation of $Mg(BH_4)_2$ for 19 h. Does not include the unchanging integrated signal intensity (9% of total boron) for the BH_3-adduct signal seen at δ = -13 ppm.

Temperature (°C)	**% $[BH_4]^-$** ***(δ = -42 ppm)***	**% $[B_3H_8]^-$** ***(δ = -31 ppm)***
23	100	0
200	97	3
210	96	4
220	94	6
230	92	8
240	90	10
250	87	13

$[BH_4]^-$. In all cases less than 20% yield of $[B_3H_8]^-$ was observed. This suggests that the conversion is equilibrium limited. In order to test this hypothesis, a sample of **1** was heated at 230 °C for 19 hours under an initial 20 bar H_2. As seen in Figure 3, this resulted in the complete suppression of

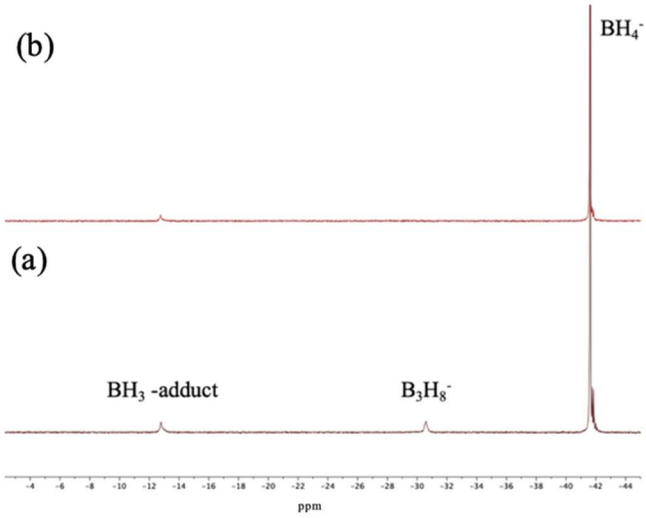

Figure 3. $^{11}B\{^1H\}$ spectra after dehydrogenation of $Mg(BH_4)_2$ (19 h, 230 °C) under **(a)** static vacuum, showing formation of 8% $[B_3H_8]^-$, and **(b)** 20 bar H_2 pressure, showing complete suppression of $[B_3H_8]^-$.

the dehydrogenation to $[B_3H_8]^-$ or any other borane products. This confirms earlier reports of the reversibility of the dehydrogenation of **1** to **3**. Figure 4 compares the isotherms obtained at 230 °C

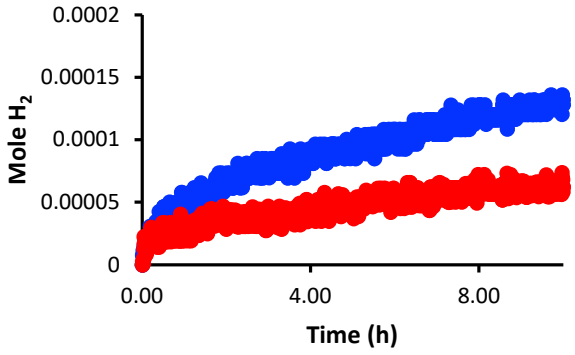

Figure 4. Isotherms of hydrogen evolution from the dehydrogenation of 100 mg of $Mg(BH_4)_2$ at 230 °C. Blue: under static vacuum. Red: under 20 bar H_2 (backpressure subtracted).

with and without backpressure of 20 bar H_2. Clearly the evolution of hydrogen is suppressed by hydrogen backpressure. This establishes that the elimination of H_2 is the rate limiting step in the dehydrogenation process. It is noted that our starting material generaly contained ≤10% of a BH_3-adduct that has been observed to be present and inert in previous studies of the dehydrogenation of $Mg(BH_4)_2$ [8,10].

Kinetic Modeling

A kinetic modeling study was undertaken in order to determine activation energies and further elucidate mechanistic details of the dehydrogenation reaction. We initially implemented a model that assumed a reversible, one-step first-order process (Figure 5). The comparison of the results

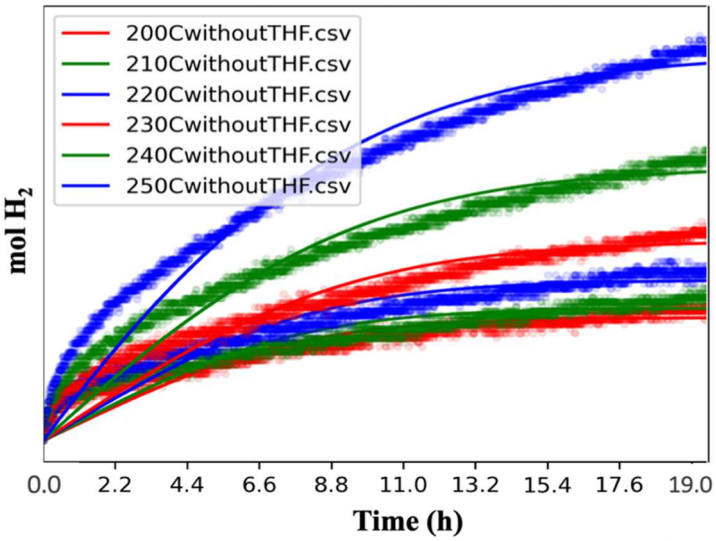

Figure 5. The progression of kinetic modeling of H_2 isotherms showing $Mg(BH_4)_2$ dehydrogenation modeled as a one-step reversible process.

of this computational model and the experimental data reveals this model to be inadequate. This suggests that the dehydrogenation of $[BH_4]^-$ to form $[B_3H_8]^-$ does not occur in a single step but

rather through a multi-step mechanism. Accordingly, a second modeling study was conducted based on the three-step reaction sequence, shown in Equations 4*a* – 4*c* that was previously found

$$2[BH_4]^- \rightleftarrows [B_2H_7]^- + [H]^- \quad \textit{(fast)} \quad (4a)$$

$$[B_2H_7]^- + [BH_4]^- \leftrightarrows [B_3H_{10}]^- + [H]^- \quad \textit{(fast)} \quad (4b)$$

$$[B_3H_{10}]^- \leftrightarrows [B_3H_8]^- + H_2 \quad \textit{(slow)} \quad (4c)$$

to be the most energetically favorable for the formation of $[B_3H_8]^-$ in the computational study by Johnson *et al* [20]. In accordance with the experimental observations, all steps are assumed to be reversible. Upon incorporation of parameters for the three-step model, a variety of solutions gave suitable fits with the experimental data as six independent rate constants give rise to a very large parameter space and many solution sets of rate constants were found. The outcome of the fitting, which corresponds to the local minimums of the cost function (i.e., the deviation between the fit and the experimentally measured amount of H_2), heavily depends on the boundaries of the parameter space. Solution limits were selected within the range of those that are known for chemical processes occuring in this temperature range. The excellent fit of computational and experimental data seen in Figure 6 was obtained using the set of compling rate constants seen in Table 2. This solution was chosen as it has hydrogen elimination as the rate determining step. Arrhenius plots of these rate constants (Figure 7) give rise to the Ea value seen in Table 2. While the absolute accuracy of the rate constants is questionable, the trends of the temperature dependance of the rate constants which are the basis of the Arrehnius plots are the same for sets of rate constants giving reasonable activation energies.

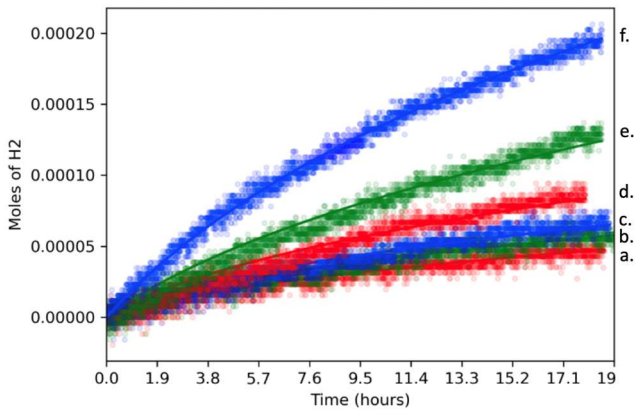

Figure 6. The progression of kinetic modeling of H_2 isotherms showing $Mg(BH_4)_2$ dehydrogenation modeled as a three step reversible process. **(a)** 200 °C **(b)** 210 °C **(c)** 220 °C **(d)** 230 °C **(e)** 240 °C **(f)** 250 °C.

Table 2. Calculated rate constants and activation energies from isotherm modeling.

	$2[BH_4]^- \rightleftarrows [B_2H_7]^- + [H]^-$		$[B_2H_7]^- + [BH_4]^- \leftrightarrows [B_3H_{10}]^- + [H]^-$		$[B_3H_{10}]^- \leftrightarrows [B_3H_8]^- + H_2$	
	k_{1f}	k_{1r}	k_{2f}	k_{2r}	k_{3f}	k_{3r}
200 ˚C	2.64	3.58E+09	5.95E+11	1.20E+07	9.31E-03	5.73E-07
210 ˚C	2.74	8.43E+09	6.58E+11	2.82E+07	1.75E-02	8.32E-07
220 ˚C	3.15	1.10E+10	8.15E+11	2.68E+07	2.14E-02	2.02E-06
230 ˚C	3.10	3.65E+10	1.07E+12	2.56E+07	3.94E-02	1.17E-05
240 ˚C	7.21	4.03E+10	2.01E+12	3.46E+07	3.89E-02	2.40E-05
250 ˚C	11.51	8.44E+10	4.17E+12	1.08E+08	9.69E-02	3.40E-04
E_a (kJ/mol)	42	127	58	41	74	203

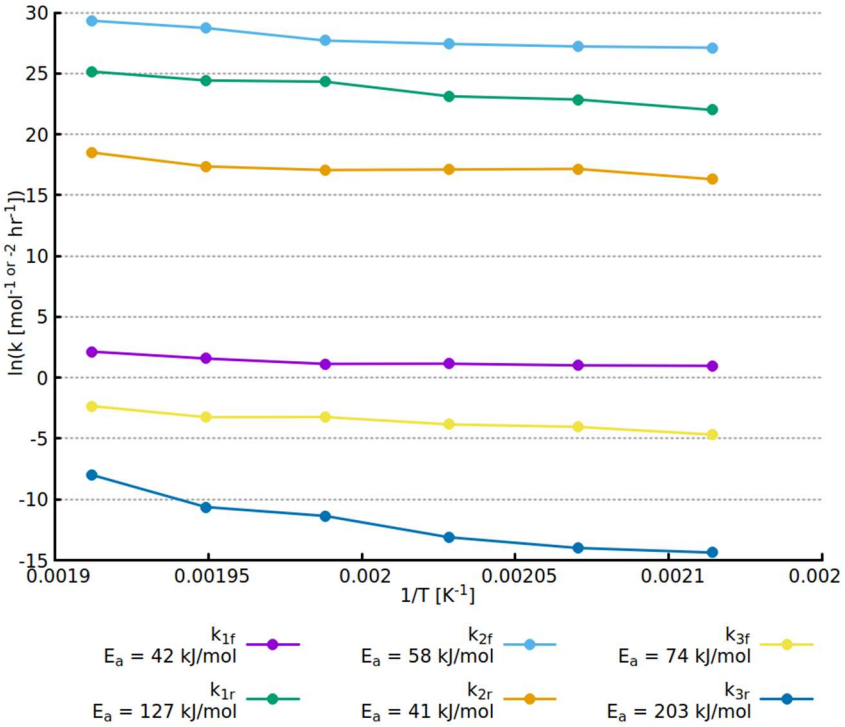

Figure 7. Arrhenius plots and calculated activation energies in the forward and reverse directions in the solid-state transformations from $[BH_4]^-$ to $[B_3H_8]^-$.

Mechanism of the Solid State Conversion of $[BH_4]^-$ to $[B_3H_8]^-$

As cautioned by Johnson *et al.* gas phase energetics are not necessarily directly comparable to those of processes occurring in the solid state [20]. Solid state reactions, unlike those occurring in solution, are often rate limited by processes involving long-range transport of heavy atoms that require large amounts of energy to produce new crystalline phases. These processes generally occur only at temperatures much higher than the 200-250 °C temperature range required for the observed dehydrogenation reaction. It is therefore important to note that in these studies, powder XRD analysis (Figure 8) of the product mixture resulting from the heating of the as synthesized

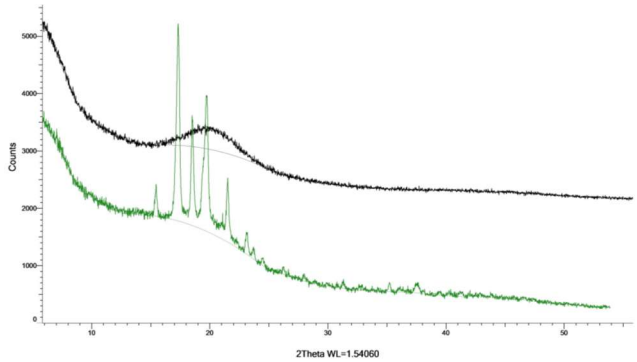

Figure 8. Powder XRD spectra of: starting material (primarily alpha) $Mg(BH_4)_2$ (green); product mixture obtained after heating at 240 °C for 12 h (black).

$Mg(BH_4)_2$ (primarily alpha phase) for 12 hours at 240 °C showed the product mixture to be totally amorphous. This observation is consistent with computational studies by Kang *et al.* indicated that $[B_3H_8]^-$ formation likely favored growth in lower dimensional morphologies such as in chains or clusters, rather than segregated crystalline phases of **2** and **1** [31]. Apparently, the $[B_3H_8]^-$ and $[H]^-$ anions formed during the course of this reaction are stabilized through complicated bonding interactions with Mg^{2+}, unreacted $[BH_4]^-$, and perhaps other species.

The formation of $[B_3H_8]^-$ can be accounted for by the reaction of neighboring groups such as seen in Scheme 2. This process involves the transfer of BH_3 to adjacent groups. These transfers are low energy processes due to the restricted movements of species within the lattice framework. Since interactions occur only between the central borohydride and its nearest neighbors, growth of the central borohydride is limited to boranes no larger than three boron atoms. The lack of detection of higher borane anions such as $[B_{10}H_{10}]^{2-}$ and $[B_{12}H_{12}]^{2-}$ in these studies is accounted for as their formation would require long-range movement of boron atoms that is not energetically possible at these temperatures.

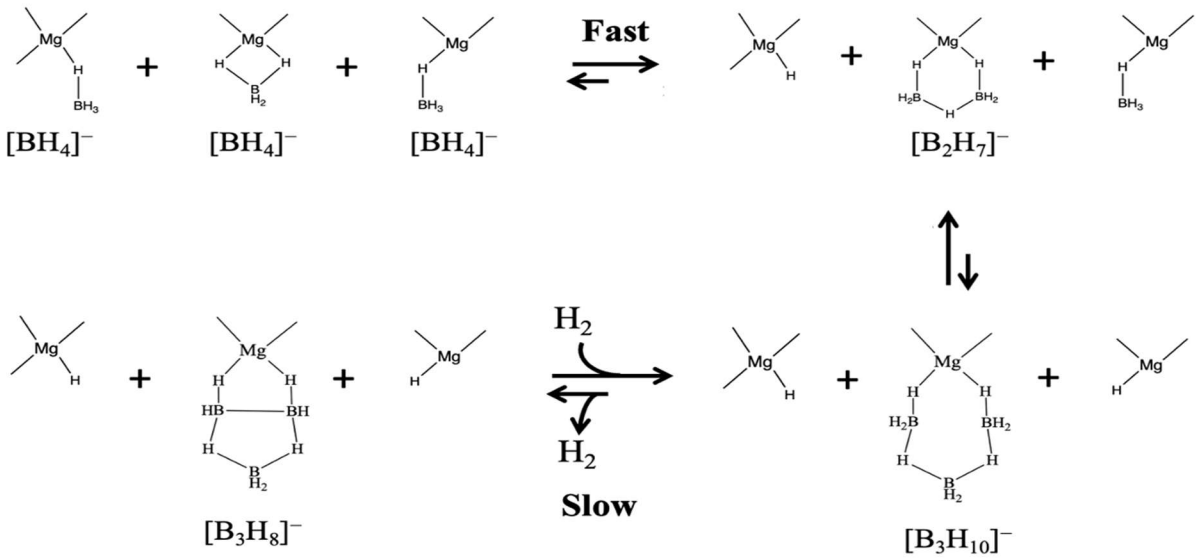

Scheme 2. The mechanism for the solid-state transformation from $[BH_4]^-$ to $[B_3H_8]^-$.

3. CONCLUSIONS

The studies reported here show that the dehydrogenation of $Mg(BH_4)_2$ to $Mg(B_3H_8)_2$ is suppressed by hydrogen pressure indicating that the rate-limiting step in this process involves hydrogen elimination. The computational work stands in agreement with the experimental observations that the reverse reactions play an important role in the overall chemical behavior of this system under moderate conditions. Overall the cost function is much higher without consideration of the reverse reactions. Numerous sets of rate constants can be obtained from the kinetic fitting with similar cost function and distinguishing them is beyond the scope of the current study. However, the kinetic fits supports the conclusion reached by a computational study by Johnson *et al.* that the dehydrogenation occurs through a three-step process and that the reversible hydrogen elimination is rate limiting. The formation of $[B_3H_8]^-$ at relatively low temperatures can be accounted for by a low energy transfer of neighboring BH_3 groups. This also explains the lack

of formation of higher borane anions under these conditions as it would require long-range movement of boron atoms.

Corresponding Author

*Craig M. Jensen, jensen@hawaii.edu

Footnotes

1. Taken in part from the PhD dissertation of Sunil Shrestha, Kinetics, Modeling and Mechanistic Analysis for the Dehydrogenation of Magnesium Borohydride. University of Hawai‘i, December 2023.

2. J.J. Zuckerman Fellow 2023.

Author Contributions

The manuscript was written through contributions of all authors. All authors have given approval to the final version of the manuscript.

Funding Sources

Pacific Northwest National Laboratory sub-contract from the US Department of Energy, Hydrogen Fuel Cell and Technologies office.

Acknowledgements

We wish to thank the Pacific Northwest National Laboratory for providing a sub-contract from funding obtained from the US Department of Energy, Hydrogen Fuel Cell and Technologies office.

The authors thank Dr. Przemyslaw Dera of the Hawaii Institute of Geophysics and Planetology at the University of Hawaii for use of the Bruker D8 powder XRD.

REFERENCES

1. S.-i.Orimo, Y. Nakamori, J. Eliseo, A. Züttel, C. M. Jensen, Complex Hydrides for Hydrogen Storage, Chem. Rev. 107 (2007) 4111-4132, https://doi.org/10.1021/cr0501846.

2. H.-W. Li, Y. Yan, S.-i. Orimo, A. Züttel, C. M. Jensen, Recent Progress in Metal Borohydrides for Hydrogen Storage, Energies 4 (2011) 185-214, https://doi.org/10.3390/en4010185.

3. L.V. Titov, Synthesis and chemical transformations of ionic octahydrotriborates. Cleavage of the $B_3H_8^-$ anion, Russian J. Inorg. Chem. 48 (2003) 1613-1623.

4. H.-W. Li, K. Kikuchi, T. Sato, Y. Nakamori, N. Ohba, M. Aoki, K. Miwa, S. Towata, S.-i. Orimo, Synthesis and Hydrogen Storage Properties of a Single-Phase Magnesium Borohydride $Mg(BH_4)_2$, Mat. Trans. 49 (2008) 2224-2228, https://doi.org/10.2320/matertrans.MA200807.

5. T. Matsunaga, F. Buchter, P. Mauron, M. Bielman, Y. Nakamori, S.-i. Orimo, N. Ohba, K. Miwa, S. Towata, A. Züttel, Hydrogen Storage Properties of $Mg[BH_4]_2$, J. Alloys Compds. 459 (2008) 583-588, https://doi.org/10.1016/j.jallcom.2007.05.054.

6. G. L. Soloveichik, Y. Gao, J. Rijssenbeek, M. Andrus, S. Kniajanski, R. C. Bowman, S.-J. Hwang, J-C. Zhao, Magnesium borohydride as a hydrogen storage material: Properties

and dehydrogenation pathway of unsolvated $Mg(BH_4)_2$, Int. J. Hydrogen Energy, 34 (2009) 916-928, https://doi.org/10.1016/j.ijhydene.2008.11.016.

7. G. Severa, E. Ronnebro, C. M. Jensen, Direct hydrogenation Direct hydrogenation of magnesium boride to magnesium borohydride: demonstration of >11 weight percent reversible hydrogen storage, Chem. Commun. 46 (2010) 421-423, http://dx.doi.org/10.1039/B921205A.

8. M. Chong, A. Karkamkar, T. Autrey, S. Orimo, S. Jalisatgi, C. M. Jensen, Reversible dehydrogenation of magnesium borohydride to magnesium triborane in the solid state under moderate conditions, Chem. Commun. 47 (2011) 1330–1332, https://doi.org/10.1039/C0CC03461D.

9. O. Zavorotynska, S. Deledda, B. C. Hauback, Recent progress in magnesium borohydride Mg(BH4)2: Fundamentals and applications for energy storage, Int. J. Hydrog. Energy 41 (2016) 9885–9892, https://doi.org/10.1016/j.ijhydene.2016.02.015.

10. M. Chong, M. Matsuo, S. Orimo, T. Autrey, C. M. Jensen, Selective Reversible Hydrogenation of $Mg(B_3H_8)_2/MgH_2$ to $Mg(BH_4)_2$: Pathway to Reversible Borane-Based Hydrogen Storage? Inorg. Chem. 54 (2015) 4120–4125, https://doi.org/10.1021/acs.inorgchem.5b00373.

11. R. J. Newhouse, V. Stavila, S-J. Hwang, L. E. Klebanoff, J. Z. Zhang, Reversibility and Improved Hydrogen Release of Magnesium Borohydride, J. Phys. Chem. C 114 (2010) 5224-5232, https://doi.org/10.1021/jp9116744.

12. B. L. Tran, T. N. Allen, M. E. Bowden, T. Autrey, C. M. Jensen, Effects of Glymes on the Distribution of $Mg(B_{10}H_{10})$ and $Mg(B_{12}H_{12})$ from the Thermolysis of $Mg(BH_4)_2$, Inorganics 9 (2021) 41, https://doi.org/10.3390/inorganics9060041.

13. M. A. N. Ahmad, N. Sazelee, N. A. Ali, M. Ismail, An Overview of the Recent Advances of Additive-Improved $Mg(BH_4)_2$ for Solid-State Hydrogen Storage Material, Energies 15 (2022) 862, https://doi.org/10.3390/en15030862.

14. N. A. Strange, N. Leick, S. Shulda, A. Schneemann, V. Stavila, A. S. Lipton, M. F. Toney, T. Gennett, S. T. Christensen, Reactive Vapor-Phase Additives toward Destabilizing γ-$Mg(BH_4)_2$ for Improved Hydrogen Release, ACS Appl. Energy Mater. 5 (2022) 1690-1700, https://doi.org/10.1021/acsaem.1c03128.

15. S. Ali, S. M. Al-Barody, T. M. B. Albarody, M. S. Nasif, E. Solangi, S. N. Al-Challabi, Progress in additive-enhanced magnesium borohydride $Mg(BH_4)_2$ for hydrogen storage applications: A systematic review, Int. J. Hydrogen Energy 92 (2024) 1172-1201, https://doi.org/10.1016/j.ijhydene.2024.10.178.

16. C. Sugai, S. Kim, G. Severa, J. L. White, N. Leick, M. B. Martinez, T. Gennett, V. Stavila, C. M. Jensen, Kinetic Enhancement of Direct Hydrogenation of MgB_2 to $Mg(BH_4)_2$ upon Mechanical Milling with THF, MgH_2, and/or Mg, ChemPhysChem 20 (2019) 1301−1304, https://doi.org/10.1002/cphc.201801187.

17. G. Severa, L. Wang, S. Kim, N. Leick, C. Kelly, C. Sugai, J. L. Snider, A. G. Norman, P. Dera, I. Kotsol, T. Gennett, V. Stavila, C. M. Jensen, Graphene Activated Magnesium Diboride for Moderate Pressure and Temperature Hydrogenation to Magnesium

Borohydride, ACS Appl. Energy Mater. 8 (2025) 853-860, https://doi.org/10.1021/acsaem.4c02302.

18. A. Gigante, N. Leick, A. S. Lipton, B. Tran, N. A. Strange, M. Bowden, M. B. Martinez, R. Moury, T. Gennett, H. Hagemann, T. S. Autrey, Thermal conversion of unsolvated $Mg(B_3H_8)_2$ to BH_4^- in the presence of MgH_2. ACS Appl. Energy Mater. 4 (2021) 3737–3747, https://doi.org/10.1021/acsaem.1c00159.

19. L. F. Wan, T. Autrey, B. C. Wood, First-Principles Elucidation of Initial Dehydrogenation Pathways of $Mg(BH_4)_2$, J. Phys. Chem. Lett. 13 (2022) 1908–1913, https://doi.org/10.1021/acs.jpclett.2c00112.

20. S. I. Johnson, J. M. DeMaria, B. Ginovska, G. M. Edvenson, H. Hagemann, T. S. Autrey, Exploring Detailed Reaction Pathways for Hydrogen Storage with Borohydrides Using DFT Calculations, Energy Fuels 36 (2022) 5513–5527, https://doi.org/10.1021/acs.energyfuels.2c00331.

21. H. C. Brown, P. A. Tierney, The Reaction of Lewis Acids of Boron with Sodium Hydride and Borohydride, J. Am. Chem. Soc. 80 (1958) 1552−1558, https://doi.org/10.1021/ja01540a011.

22. H. C. Miller, N. E. Miller, E. L. Muetterties, Chemistry of boranes. XX. Syntheses of polyhedral boranes, Inorg. Chem. 3 (1964) 1456−1463, https://doi.org/10.1021/ic50020a026.

23. K. Hoang, C. G. Van de Walle, Mechanism for the decomposition of lithium borohydride, Int. J. Hydrogen Energy 37 (2012) 5825–5832, https://doi.org/10.1016/j.ijhydene.2012.01.002.

24. W. G. Evans, C. E. Holloway, K. Sukumarabandhu, D. H. McDaniel, Strong hydrogen bonds. IV. The $B_2H_7^-$ species, Inorg. Chem. 7 (1968) 1746–1748, https://doi.org/10.1021/ic50067a011.

25. H. Beall, D. F. Gaines, Mechanistic aspects of boron hydride reactions, Inorganica Chim. Acta 289 (1999) 1–10, https://doi.org/10.1016/S0020-1693(99)00053-5.

26. X-M. Chen, N. Ma, Q. F. Zhang, J. Wang, X. Feng, C. Wei, L. S. Wang, J. Zhang, X. Chen, Elucidation of the Formation Mechanisms of the Octahydrotriborate Anion ($B_3H_8^-$) through the Nucleophilicity of the B–H Bond, J. Am. Chem. Soc. 140 (2018), 6718–6726, https://doi.org/10.1021/jacs.8b03785.

27. G. B. Dunks, K. Barker, E. Hedaya, C. Hefner, K. Palmer-Ordonez, P. Remec, Simplified synthesis of decaborane(14) from sodium tetrahydroborate via tetradecahydroundecaborate(1-) ion, Inorg. Chem. 20 (1981) 1692–1697, https://doi.org/10.1021/ic50220a015.

28. D. F. Gaines, R. Schaeffer, F. Tebbe, Convenient Preparations of Solutions Containing the Triborohydride Ion, Inorg. Chem. 2 (1963) 526–528, https://doi.org/10.1021/ic50007a025.

29. W. N. Lipscomb, Boron Hydrides, Dover Publications Inc. New York, (2012) ISBN: 9780486488226.

30. P. Zanella, L. Crociani, N. Masciocchi, G. Giunchi, Facile High-Yield Synthesis of Pure, Crystalline $Mg(BH_4)_2$, Inorg. Chem. 46 (2007) 9039−9041, https://doi.org/10.1021/ic701436c.

31. S. Kang, T. W. Heo, M. D. Allendorf, B. C. Wood, Morphology-Dependent Stability of Complex Metal Hydrides and Their Intermediates Using First-Principles Calculations, ChemPhysChem 20 (2019) 1340–1347, https://doi.org/10.1002/cphc.201801132.